Geophysical Research Letters

RESEARCH LETTER
10.1029/2025GL115255

Predicting CO Cameron-Band Auroral Emission at Venus Using VEx Electron Observations

Shaosui Xu[1], Rudy A. Frahm[2], Yingjuan Ma[3], David L. Mitchell[1], Janet G. Luhmann[1], Jean-Claude Gérard[4], Lauriane Soret[4], and Robert J. Lillis[1]

[1]Space Sciences Laboratory, University of California, Berkeley, CA, USA, [2]Southwest Research Institute, San Antonio, TX, USA, [3]Department of Earth Planetary and Space Sciences, University of California, Los Angeles, CA, USA, [4]Laboratoire de Physique Atmosphérique et Planétaire (LPAP), STAR Institute, Université de Liège, Liège, Belgium

Key Points:

- We predict the possible CO Cameron-band emission brightness at Venus using VEx electron observations by applying an empirical relationship
- To reproduce PVO observations, electron acceleration is not needed, but magnetic topology limits the occurrence of aurorae at Venus
- Auroral imaging at Venus can serve as remote sensing of the magnetic state of the Venus nightside ionosphere and magnetosphere

Correspondence to:
S. Xu,
shaosui.xu@ssl.berkeley.edu

Citation:
Xu, S., Frahm, R. A., Ma, Y., Mitchell, D. L., Luhmann, J. G., Gérard, J.-C., et al. (2025). Predicting CO Cameron-band auroral emission at Venus using VEx electron observations. *Geophysical Research Letters*, *52*, e2025GL115255. https://doi.org/10.1029/2025GL115255

Received 5 FEB 2025
Accepted 31 MAR 2025

Abstract Various types of auroral emissions have been observed at (partially) magnetized planets (e.g., Earth, Jupiter, and Mars). Auroral emissions have also been observed at Venus, an unmagnetized planet, by the Pioneer Venus Orbiter (PVO) and ground-based telescopes. By applying a linear relation, this study predicts the possible CO Cameron-band emission brightness at Venus using electron observations from Venus Express (VEx). Our results suggest that to produce the PVO observations, electron acceleration is not required as in the case of discrete aurorae at magnetized planets; rather, the magnetic access of precipitating electrons to the lower atmosphere is the more limiting factor for auroral occurrence. This study helps better understand how aurorae can occur at an unmagnetized planet, in contrast to magnetized planets. It also has implications for future Venus mission design: auroral imaging can serve as a remote sensing tool to characterize the magnetization state of the Venus nightside atmosphere.

Plain Language Summary Auroral emissions have been observed (partially) magnetized planets, such as Earth, Jupiter, and Mars, illuminating the plasma processes mostly related to planetary intrinsic fields. Aurorae have also been reported to occur at Venus, an unmagnetized planet, by the Pioneer Venus Orbiter (PVO). Previous modeling efforts suggest that the observed CO Cameron-band auroral emissions are mainly produced by electrons at 10–100s of electron volts (eV) impacting the Venus nightside upper atmosphere. Yet, little was discussed in previous studies regarding how these source electrons access the atmosphere. By applying a linear relation, this study predicts the possible CO Cameron-band emission brightness at Venus using electron observations from Venus Express (VEx). Our results suggest that to produce the PVO observations, electron acceleration is not required as in the case of discrete aurorae at magnetized planets; rather, the magnetic access of precipitating electrons to the lower atmosphere is the more limiting factor for auroral occurrence. This study helps better understand how aurorae can occur at an unmagnetized planet, in contrast to magnetized planets. It also has implications for future Venus mission design: auroral imaging can serve as a remote sensing tool to characterize the magnetization state of the Venus nightside atmosphere.

1. Introduction

Auroral emissions have been observed at Venus by Pioneer Venus Orbiter (PVO) (Fox & Stewart, 1991; Gérard et al., 2008; Phillips et al., 1986) and also by ground-based telescopes (Gray et al., 2014). More specifically, the ground-based observations of the Venus nightside emission are the 557.7-nm oxygen green line, which is highly temporally variable and strongly correlated with solar events (solar flares, coronal mass ejections, and solar wind streams) (Gray et al., 2014, 2025). The speculated main source particles for this type of emission are solar energetic particles (SEPs). The auroral emissions observed by the Pioneer Venus Orbiter Ultraviolet Spectrometer (PV-OUVS) include 130.4, 135.6 nm, and CO Cameron band emissions (Fox & Stewart, 1991; Phillips et al., 1986). The observed 130.4-nm emission is reported to be highly variable, both spatially (bright spots) and temporarily (varying from orbit to orbit) (Phillips et al., 1986). The CO Cameron-band emissions are less well-characterized and are only reported to exist. These bands have been shown to have a brightness of 25 ± 50 R (e.g., Gérard et al., 2008). Simulations have suggested that soft (sub-keV) electrons, such as ionospheric photoelectrons and solar wind electrons, have sufficient energy fluxes to produce the PVO auroral emissions (Fox & Stewart, 1991; Gérard et al., 2008).

In previous work, little attention was paid to how the source electrons of auroral emissions access the collisional atmosphere at Venus. As sub-keV and keV electrons are generally magnetized at Venus, these electrons have to

be on magnetic field lines connected to the nightside atmosphere to cause auroral emission. Venus's induced magnetosphere comprises the impinging interplanetary magnetic field (IMF) draped around the planet. The IMF can penetrate deeply into the collisional ionosphere during periods of high upstream solar wind dynamic pressures and/or low solar extreme ultraviolet (EUV) intensities (e.g., Luhmann, 1986; Luhmann & Cravens, 1991; Luhmann et al., 1981). Magnetic topology can be defined as the magnetic connectivity between Venus's collisional ionosphere (more specifically, the superthermal electron exobase at ∼200 km altitude at Venus (Butler & Stolarski, 1978; Xu et al., 2016)) and the solar wind. Magnetic topology characterizes the magnetization state of the Venus ionosphere and also offers a necessary piece of information for auroral emissions, that is, the magnetic connectivity to the nightside collisional atmosphere.

Magnetic connectivity to the collisional atmosphere can be inferred from (a) the presence of loss cones in the electron pitch angle distribution (e.g., Brain et al., 2007; Weber et al., 2017; Xu et al., 2024), indicative of superthermal electrons being absorbed by the collisional atmosphere; and (b) the presence of ionospheric photoelectrons (only produced in the dayside ionosphere), indicative of magnetic connectivity to the dayside ionosphere (e.g., Coates et al., 2011; Frahm et al., 2006; Xu et al., 2017, 2019). Combining both types of information, magnetic topology can be categorized into six subtypes at Venus (Xu et al., 2021, 2023, 2024) based on being magnetically connected to the dayside and/or nightside collisional atmosphere: (a) "closed-to-day" (C-D) with dayside connectivity on both ends, (b) "cross-terminator-closed" (C-X) with one footpoint on the dayside and the other on the nightside, (c) "closed-to-night" (C-N) with only nightside connectivity on both ends, (d) "open-to-day" (O-D) connected to the dayside on one end and to the solar wind on the other end, (e) "open-to-night" (O-N) connected to the nightside on one end and to the solar wind on the other end, and (f) draped (DP) with no connectivity to the collisional atmosphere. Xu et al. (2023) conclude that the draped topology is the dominant topology in the near-Venus space environment, >70%, except at low altitudes close to the ionosphere. Open topology makes up 20%–30% of the magnetotail and at low altitudes. More interestingly, there is an occurrence rate up to ∼10% and ∼20% for the closed-to-day (C-D) and cross-terminator-closed (C-X) topologies, respectively (Xu et al., 2023), surprising magnetic structures at Venus first reported by Xu et al. (2021). Lastly, Xu et al. (2024) report closed loops connected only to the nightside (C-N) in the Venus magnetotail, but no significant reoccurrence of this topology is found thus far (Xu et al., 2023).

For an observable auroral emission event, two conditions are necessary: source electrons (a) have pathways to precipitate onto the collisional atmosphere and (b) have sufficient energy fluxes to produce a brightness surpassing the instrument detection threshold. As illustrated in Figure 1, two magnetic topologies can supply source electrons to the nightside atmosphere to cause auroral emissions: (a) ionospheric photoelectrons transported to the nightside atmosphere via cross-terminator-closed (C-X) magnetic field lines and (b) solar wind electrons precipitating onto the nightside atmosphere via open-to-night (O-N) magnetic field lines. Meanwhile, Xu et al. (2022) empirically established a linear relation between auroral electron energy fluxes and the CO Cameron-band emissions using the combination of auroral observations and superthermal electron observations from the Mars Atmospheric Volatile EvolutioN (MAVEN) mission. As the dominant neutral species for Mars and Venus is CO_2 at superthermal electron deposition altitudes (∼< 150 km) (Hedin et al., 1983; Martinez et al., 2023), the main production process of the CO Cameron-band emissions would be electrons impacting CO_2, in comparison to electrons impacting CO. While the peak emission altitude is expected to differ between Venus and Mars because of their different CO_2 density profiles, the column-integrated emission should be similar given the same source electrons. In other words, to the first approximation, we can apply the linear relation obtained at Mars to Venus to estimate the expected CO Cameron-band emission brightness for a given electron energy flux.

In this study, we utilize superthermal electron and magnetic field measurements from the Venus Express (VEx) mission (Svedhem et al., 2007) to infer magnetic topology and to derive the expected auroral brightness from the measured energy fluxes of precipitating source electrons. We then statistically quantify the detection probability and determine whether ionospheric photoelectrons and solar wind electrons could be the source electrons for the auroral emissions observed by PVO. This paper is organized as follows: Section 2 describes the instrument and data; Section 3 presents our main results; we then conclude the study in Section 4.

2. Methodology

Data used in this study include magnetic fields measured by the Magnetometer (MAG) (Zhang et al., 2006), and electron energy and pitch angle distributions measured by the Electron Spectrometer (ELS) of the Analyser of

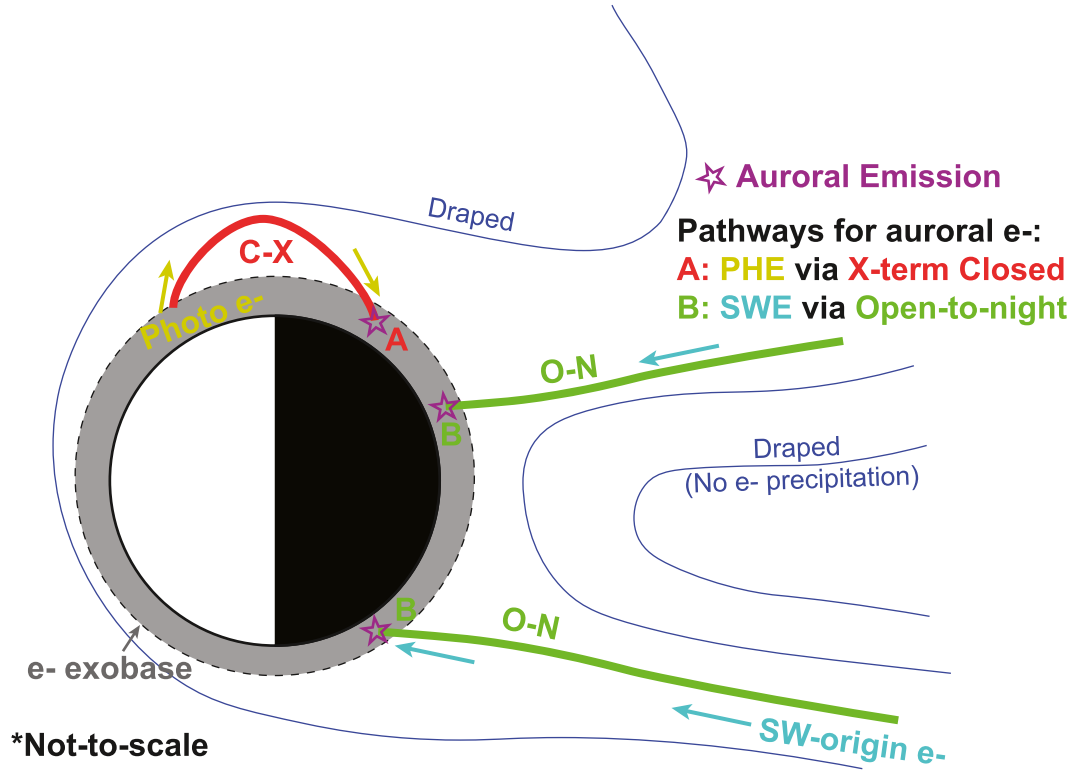

Figure 1. A schematic shows the two possible pathways for precipitating electrons to produce auroral emissions (i.e., auroral electrons) at Venus: (a) photoelectron (PHE) precipitation via cross-terminator (C-X) closed field lines and (b) solar wind electron (SWE) precipitation via open-to-night (O-N) field lines. The dashed thin circle indicates the superthermal electron exobase, which is slightly above the auroral emission altitudes (marked by purple stars).

Space Plasmas and Energetic Atoms-4 (ASPERA-4) instrument suite (Barabash et al., 2007) on VEx. The MAG instrument consists of two triaxial flux gate sensors, providing magnetic vectors at a time cadence of 1 or 4 s. The ELS instrument is an axially symmetric spherical top-hat analyzer that has an energy resolution (ΔE/E, FWHM) of 9% and measures an energy range of 0.8 eV–30 keV (0.8–200 eV) with 127 (31) energy steps every ~4s (1s). The instrument has a limited field of view (FOV) of 360° × 4°, corresponding to a 2-D "slice" through the full sky.

Magnetic topology used in this study is inferred using the methodology described in Xu et al. (2023), with a main focus on cross-terminator-closed (C-X) field lines and open-to-night (O-N) field lines. Another parameter calculated in this study is the integrated electron energy flux I_e in units of eV cm^{-2} s^{-1} sr^{-1}, which is the differential energy flux first averaged over a pitch angle (PA) range of 0−60° or 120 − 180° and then integrated over an energy range of 20–2,000 eV. The choice of PA 0 − 60° or 120−180° is made based on the local magnetic elevation angle such that the fluxes for electrons traveling toward the planet are chosen. We use a lower energy bound of 20 eV, rather than 50 eV as in Xu et al. (2022), because Xu et al. (2022) focus on accelerated electrons, while this study explores a broader energy range to include unaccelerated electrons. More specifically, a cutoff of 20 eV is used as the excitation cross section of the CO Cameron bands by electron impact on CO_2 peaks at about 20 eV, below which the excitation cross is quite small (Gérard et al., 2023). As spacecraft potential estimates are not available for VEx but are expected to be of order −10 V in darkness, this energy cutoff reduces the impact of not correcting electron fluxes for spacecraft potential.

The scale factor from integrated electron fluxes I_e (in units of eV cm^{-2} s^{-1} sr^{-1}) to the CO Cameron brightness (EB_{CO} in Rayleigh) used in Xu et al. (2022) is $I_e = 4.4 \times 10^6\ EB_{CO}$ (after correction), which applies to electrons with a characteristic energy of order 100 eV. Note that the scaling factor in Xu et al. (2022), $I_e = 2.2 \times 10^7\ EB_{CO}$, was a factor of 5 too high because of an error in their calculation of electron flux integration and has been revised. Model results predict a factor of 1.7 enhancement in EB_{CO} with a primary electron

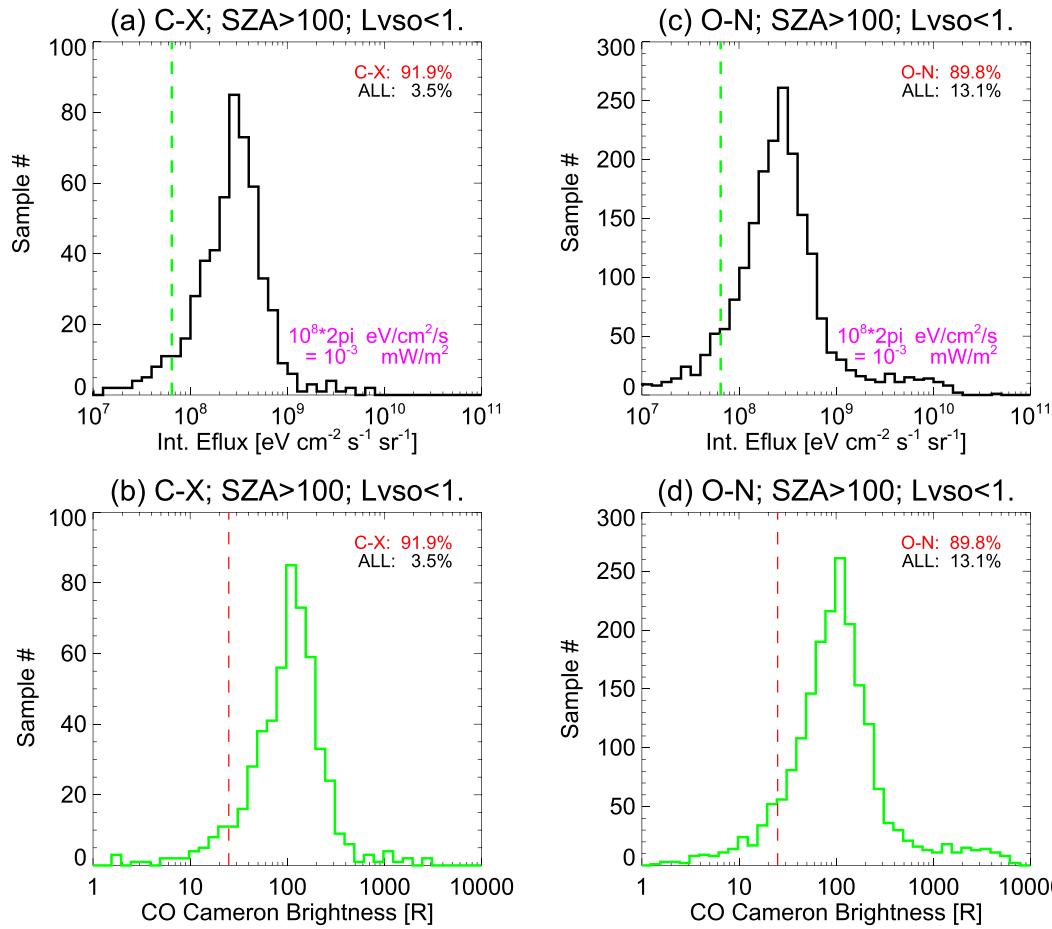

Figure 2. The distribution (number of samples) of I_e (in units of eV cm^{-2} s^{-1} sr^{-1}) (a, c) and the correspondingly inferred EB_{CO} (in R) (b, d) for cross-terminator-closed (C-X) field lines (a, b) and open-to-night (O-N) field lines (c, d). The sampling region is limited to SZA>100° and $L_{V\,SO} < 1\ R_V$ for all panels. The green dashed lines in panels a and c mark the electron flux thresholds for an auroral emission brightness threshold of $EB_{CO} = 25$ R. The red dashed lines in panels b and d mark the observed auroral brightness of 25 R by PVO. The occurrence rates on the upper right corner of each panel are p_e^{CX} (red, panels a, b), p_e^{ON} (red, panels c, d), p_t^{CX} (black, panels a, b), and p_t^{ON} (black, panels c, d). See definitions in the text.

energy of 20 eV in comparison to 100 eV (Gérard et al., 2023). Therefore, the linear scale used in this study is $I_e = 2.6 \times 10^6\ EB_{CO}$. It is also worth noting that I_e is differential fluxes per steradian, and a solid angle should be applied to obtain the total electron energy flux. At Venus, the loss cone size is typically around 45° to 90°, which corresponds to a solid angle of $\sim 1.4\pi - 2\pi$.

The main coordinate system used in this study is the Venus-Solar-Orbit (VSO) frame, where the *X*-axis points from the center of Venus to the Sun, the *Y*-axis points opposite to Venus's orbital motion, and the *Z*-axis points to the north pole of the Venus elliptical plane. A cylindrical length $L_{V\,SO}$ is calculated as $L_{V\,SO} = \sqrt{Y_{V\,SO}^2 + Z_{V\,SO}^2}$. As auroral emission is expected to occur on the nightside, we limit the spatial coverage of sampling to $L_{V\,SO} < 1\ R_V$ (within the optical shadow) and $SZA > 100°$, where R_V is the Venus radius and SZA is the solar zenith angle.

3. Results

Our results include VEx/ELS observations from May 2006 to November 2014. Figures 2a and 2c show the distributions of the integrated electron energy fluxes I_e on cross-terminator-closed (C-X) field lines and open-to-night (O-N) field lines, respectively, limited to $L_{V\,SO} < 1\ R_V$ and $SZA > 100°$. In principle, the source electrons on

Table 1
Summary of Sampling Numbers and Occurrence Rates

Topology type	Sample # of topology (N)	N_{ae}	N_{tot}	$p_e = N_{ae}/N$ (%)	$p_t = N_{ae}/N_{tot}$ (%)
Cross-terminator closed (C-X)	534	491	13,877	91.9	3.5
Open-to-night (O-N)	2,018	1,813	13,877	89.8	13.1

the C-X topology are ionospheric photoelectrons, and the source electrons on the O-N topology are solar-wind-origin electrons. The two distributions in panels a and c are very similar, with most of I_e ranging $10^8 - 10^9$ eV cm^{-2} s^{-1} sr^{-1}, equivalent to $10^{-3} - 10^{-2}$ mW m^{-2} with a solid angle of 2π being applied. There is a small tail of $I_e > 10^9$ eV cm^{-2} s^{-1} sr^{-1} on O-N field lines (Figure 2c), probably a result of some tail electron acceleration processes.

We apply the scaling function, $I_e = 2.6 \times 10^6\ EB_{CO}$, to the electron flux distributions in Figures 2a and 2c to obtain the expected distributions of the CO Cameron brightness EB_{CO} (in R) for the C-X and O-N topology, shown in Figures 2b and 2d, respectively. The derived EB_{CO} mostly ranges from tens to hundreds of Rayleighs, with a small fraction exceeding 1 kR on the O-N field lines. The CO cameron-band brightness from the PVO observation is around 25 ± 50 R (Fox & Stewart, 1991; Gérard et al., 2008; Phillips et al., 1986), which corresponds to $I_e = 6.5 \times 10^7$ eV cm^{-2} s^{-1} sr^{-1} (or 6.5×10^{-4} mW m^{-2} if 2π applied), marked as the green dashed lines in panels a and c.

We calculate the occurrence rates of $EB_{CO} \geq 25$ R as:

$$p_e^{CX} = \frac{N_{ae}^{CX}}{N_{CX}} \tag{1}$$

$$p_e^{ON} = \frac{N_{ae}^{ON}}{N_{ON}} \tag{2}$$

$$p_t^{CX} = \frac{N_{ae}^{CX}}{N_{tot}} \tag{3}$$

$$p_t^{ON} = \frac{N_{ae}^{ON}}{N_{tot}} \tag{4}$$

where N_{ae}^{CX} and N_{ae}^{ON} are the number of electron samples producing $EB_{CO} \geq 25$ R on the C-X and O-N topology, respectively, N_{CX} and N_{ON} are the number of the C-X and O-N topology samples, respectively, and N_{tot} is the total sample number for all I_e and topologies. p_e represents the occurrence rate of precipitating electrons producing $EB_{CO} \geq 25$ R on a specific topology, while p_t represents the overall occurrence rate of $EB_{CO} \geq 25$ R, factoring in the occurrence rate of each topology. These occurrence rates are shown in the upper right corner of each panel of Figure 2 and Table 1.

Overall, there is a probability of ~90% (p_e) for precipitating photoelectrons or solar wind electrons having sufficient energy fluxes to produce $EB_{CO} \geq 25$ R on C-X field lines or O-N field lines; however, the overall probability (p_t) is down to 3.5% and 13.1%, respectively. This is because the occurrence rates of C-X field lines and O-N field lines are very low. That is, in terms of the possibility of producing the PVO auroral observations, the nominal photoelectrons or solar wind electrons have sufficient energy fluxes, but the magnetic access of precipitating electrons to the collisional atmosphere is more of a limiting factor for aurora occurrence (but not the brightness). However, when aurora does occur, the typical auroral brightness is of order 100 R, brighter than the 25 ± 50 R seen by PV-OUVS.

The inferred EB_{CO} distribution, representing the nominal brightness distribution and range occurring at Venus, is informative of future auroral instrument design in terms of the detection threshold requirement and the detection probability. More specifically, we can calculate the accumulative probability of CO Cameron-band auroral emission detection as a function of the detection threshold (D_{Th}) of a given instrument as $\sum N_{ae}(EB_{CO} > D_{Th})/N_{tot}$, separately for the C-X (Figure 3a) and O-N (Figure 3b) topology. In the case of the C-X

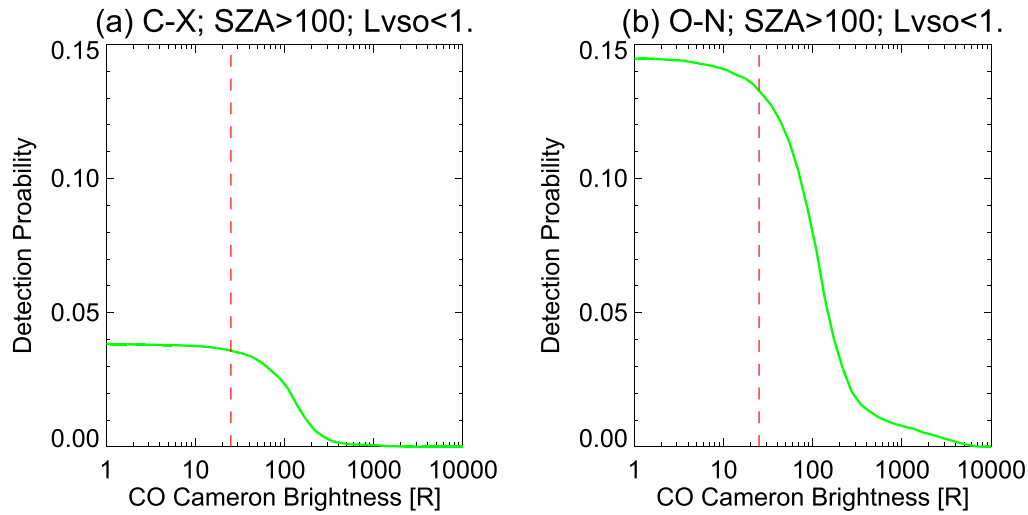

Figure 3. The accumulative probability of CO Cameron-band auroral emission detection as a function of the detection threshold separately for the C-X (a) and O-N (b) topology. The red dashed lines mark 25 R.

topology (Figure 3a), the detection probability is near 0 for an emission detection threshold of $D_{Th} > \sim 200\ R$, rapidly increases when D_{Th} is tens of Rayleighs, and reaches a maximum of ~4% for $D_{Th} < 20\ R$. Similarly, in the case of the O-N topology (Figure 3b), the detection probability is <2% for $D_{Th} > \sim 200\ R$, rapidly increases for $\sim 20 < D_{Th} < \sim 200\ R$, and peaks at ~14%. The peak probabilities correspond to the overall occurrence rate for each topology. In other words, increasing the instrument sensitivity in the range of ~20–200 R is most efficient in maximizing the CO Cameron-band auroral detection at Venus.

The results above combine all the spatial sampling by VEx. It is informative to determine the spatial distribution of the occurrence rates of auroral emissions. Here, we use $EB_{CO} = 25\ R$ as the detection threshold to calculate p_t^{CX} and p_t^{ON} in the three VSO projections, as shown in Figure 4. In the case of the C-X topology (panels a–c), p_t^{CX} is higher at regions closer to the planet, up to 6%–10%, as this topology mostly clusters near the terminator region (Xu et al., 2023). In the case of the O-N topology (panels d–f), p_t^{ON} is more or less uniform, about 10%–20%, along the X-axis. There is a noticeable dawn-dusk asymmetry in p_t^{ON}, exhibiting a higher occurrence in the $-Y_{V\,SO}$/dusk side than in the $+Y_{V\,SO}$/dawn side (Venus retrograde rotation taken into account). This might be related to the preferential precipitation of the anti-sunward solar wind strahl population on the $-Y_{V\,SO}$/dusk side, assuming a Parker spiral upstream IMF configuration. Similarly, Phillips et al. (1986) interpreted their four brightest 130.4-nm emissions all occurring at the evening sector (Figure 4 of Phillips et al. (1986)) observed by PVO as a result of the dusk side $(-Y_{V\,SO})$ being magnetically connected to the Sun.

4. Discussion and Conclusions

CO Cameron-band emission has been observed by PVO on the Venus nightside at a brightness level of 25 ± 50 R. Both ionospheric photoelectrons and solar wind electrons are hypothesized and modeled to have sufficient energy fluxes to reproduce this emission observation. This study utilizes a linear scaling between the electron energy flux and CO Cameron-band emission brightness (EB_{CO}) to empirically derive the expected auroral emission brightness at Venus from the electron observations made by the Venus Express mission. We also investigate how magnetic topology, or the pathways for source auroral electrons, contributes to the occurrence of auroral emissions, including ionospheric photoelectrons transported to the nightside via cross-terminator closed (C-X) field lines and solar wind electrons precipitating onto the nightside atmosphere via open-to-night (O-N) field lines. By examining the two topologies separately, we quantitatively assess the relative contributions of photoelectrons and solar wind electrons to Venus's auroral emissions. The derived CO Cameron-band emission brightness for both topology cases ranges from 10 to 100s R, which matches well with the PVO observations.

We further calculate the occurrence rates of electron observations producing $EB_{CO} > 25\ R$ on the C-X or O-N field lines (p_e) to be ~90%, which means nominal photoelectrons and solar wind electrons (without additional

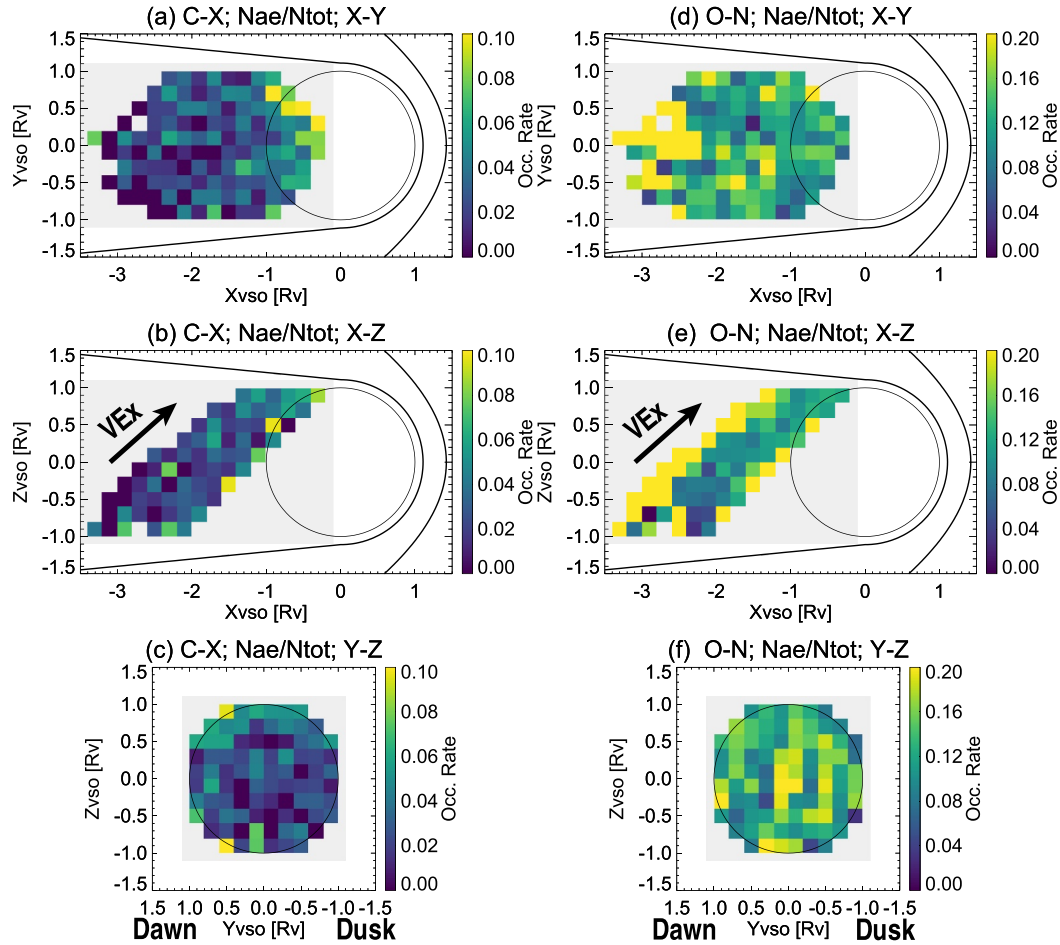

Figure 4. The overall occurrence rates of auroral electron/emission detections, (a–c) N_{ae}^{CX}/N_{tot} and (d–f) N_{ae}^{ON}/N_{tot}, mapped in different VSO projections: (a, d) $X_{V\,SO} - Y_{V\,SO}$, (b, e) $X_{V\,SO} - Z_{V\,SO}$, and (c, f) $Y_{V\,SO} - Z_{V\,SO}$. A scaling factor of $I_e = 2.6 \times 10^6\ EB_{CO}$ and a detection threshold of $EB_{CO} = 25$ R are used. Panels c and f are viewing from the tail toward the Sun.

acceleration) could be the source electrons for the observed emissions by PVO. Meanwhile, the overall occurrence rates p_t (factoring in the probability of each topology) are down to 3.5% and 13.1% on average, locally up to 6%–10% and 10%–20%, for the C-X and O-N field lines, respectively. It means that the total occurrence rate of $EB_{CO} > 25\ R$ at Venus is ∼17%, locally up to ∼30%, and also that solar wind electrons are more likely to be the source electrons than photoelectrons from the dayside ionosphere. In terms of spatial variability, p_t is higher near the terminator than further down the tail for the case of the C-X topology, and there is a dawn–dusk asymmetry in p_t for the case of the O-N topology. Comparing p_e and p_t, it means photoelectrons or solar wind electrons do not need to get energized to produce the PVO emission observation, unlike the case of discrete aurorae at Earth (e.g., Birn et al., 2012), Jupiter (e.g., Mauk et al., 2017; Mauk et al., 2020), or Mars (e.g., Brain et al., 2006; Gérard et al., 2015; Leblanc et al., 2008; Soret et al., 2016, 2021; Xu et al., 2020, 2022). In fact, as indicated by simulation results from Gérard et al. (2008), soft electrons at tens of eV are not significantly attenuated in energy fluxes at the O-dominated region and can reach the CO_2-dominated region, producing an emission rate peak at ∼140 km altitude. Instead, the magnetic access of precipitating electrons to the collisional atmosphere is the more important factor in determining the auroral occurrence/detectability in the case of Venus.

We note a few caveats in this study. First, applying the linear scaling function obtained from Mars to Venus only yields the first order of characterization of auroral emission brightnesses at Venus, as our main focus is to assess whether observed energy fluxes of photoelectrons or solar wind electrons can explain the PVO observations. A more accurate estimation requires detailed simulations using observed electron energy distribution as inputs but is

beyond the scope of this study. Second, we note that VEx experienced a weaker solar cycle, especially in terms of the solar maximum phase, than PVO. Both the occurrence rates of magnetic topology and photoelectron fluxes have a dependence on the solar cycle. Using the VEx electron observations to reproduce PVO auroral emission observations might bear such complications, but is not quite an issue for our results taken as a first approximation. Third, electron observations made by VEx are at altitudes higher than 350 km (the periapsis altitude), which is above the expected emission altitude, such that the VEx observations cannot capture possible electron acceleration below the spacecraft, if any. Additionally, as the electron measurements are made at high altitudes, it is difficult to trace down to the footpoints of the field lines and accurately determine where auroral emission occurs.

Apart from addressing the PVO auroral observations, our study also has important implications for future Venus instrument/mission designs. Our results suggest increasing the instrument sensitivity in the range of $\sim 20 - 200\ R$ is most efficient in maximizing the CO Cameron-band auroral detection at Venus. Furthermore, for an instrument sensitive enough (such as PV-OUVS) to detect almost all emission brightnesses produced by nominal photoelectrons or solar wind electrons, the auroral images serve as a remote sensing tool to characterize the magnetization state of the nightside ionosphere and magnetosphere, that is, the footpoints of the cross-terminator closed field lines and the open-to-night field lines. This type of global imaging of the magnetization of the nightside ionosphere is particularly useful for Venus as it is difficult for orbiters at Venus to make low-altitude in situ observations globally. This is important for better understanding the Sun-Venus interaction as well as searching for possible intrinsic fields of Venus.

Data Availability Statement

Venus Express Magnetometer and ELS data are publicly available in the ESA Planetary System Archive (https://www.cosmos.esa.int/web/psa/venus-express). The Pitch Angle Distribution (PAD) data from the Electron Spectrometer (ELS) instrument are publicly available at Planetary Data System: https://pds-ppi.igpp.ucla.edu/bundle/urn:nasa:pds:vex-aspera4-els-pad.

Acknowledgments

S. Xu, R. A. Frahm, and Y. J. Ma gratefully acknowledge support from NASA's Solar System Working Program, Grant 80NSSC21K0151. L. Soret is supported by the Belgian national fund for scientific research (F.R.S.-FNRS).

References

Barabash, S., Sauvaud, J.-A., Gunell, H., Andersson, H., Grigoriev, A., Brinkfeldt, K., et al. (2007). The Analyser of Space Plasmas and Energetic Atoms (ASPERA-4) for the Venus Express mission. *Planetary and Space Science*, *55*(12), 1772–1792. https://doi.org/10.1016/j.pss.2007.01.014

Birn, J., Artemyev, A., Baker, D., Echim, M., Hoshino, M., & Zelenyi, L. (2012). Particle acceleration in the magnetotail and aurora. *Space Science Reviews*, *173*(1–4), 49–102. https://doi.org/10.1007/s11214-012-9874-4

Brain, D., Halekas, J., Peticolas, L., Lin, R., Luhmann, J., Mitchell, D., et al. (2006). On the origin of aurora on Mars. *Geophysical Research Letters*, *33*(1). https://doi.org/10.1029/2005gl024782

Brain, D., Lillis, R., Mitchell, D., Halekas, J., & Lin, R. (2007). Electron pitch angle distributions as indicators of magnetic field topology near Mars. *Journal of Geophysical Research: Space Physics 1978–2012*, *112*(A9). https://doi.org/10.1029/2007ja012435

Butler, D. M., & Stolarski, R. S. (1978). Photoelectrons and electron temperatures in the Venus ionosphere. *Journal of Geophysical Research: Space Physics (1978–2012)*, *83*(A5), 2057–2065. https://doi.org/10.1029/ja083ia05p02057

Coates, A. J., Tsang, S., Wellbrock, A., Frahm, R., Winningham, J., Barabash, S., et al. (2011). Ionospheric photoelectrons: Comparing Venus, Earth, Mars and Titan. *Planetary and Space Science*, *59*(10), 1019–1027. https://doi.org/10.1016/j.pss.2010.07.016

Fox, J. L., & Stewart, A. (1991). The Venus ultraviolet aurora: A soft electron source. *Journal of Geophysical Research*, *96*(A6), 9821–9828. https://doi.org/10.1029/91ja00252

Frahm, R., Winningham, J., Sharber, J., Scherrer, J., Jeffers, S., Coates, A., et al. (2006). Carbon dioxide photoelectron energy peaks at Mars. *Icarus*, *182*(2), 371–382. https://doi.org/10.1016/j.icarus.2006.01.014

Gérard, J.-C., Hubert, B., Shematovich, V., Bisikalo, D., & Gladstone, G. (2008). The Venus ultraviolet oxygen dayglow and aurora: Model comparison with observations. *Planetary and Space Science*, *56*(3–4), 542–552. https://doi.org/10.1016/j.pss.2007.11.008

Gérard, J.-C., Soret, L., Hubert, B., Neary, L., & Daerden, F. (2023). The brightness of the CO Cameron bands in the Martian discrete aurora: A study based on revised cross sections. *Icarus*, *402*, 115602. https://doi.org/10.1016/j.icarus.2023.115602

Gérard, J.-C., Soret, L., Libert, L., Lundin, R., Stiepen, A., Radioti, A., & Bertaux, J.-L. (2015). Concurrent observations of ultraviolet aurora and energetic electron precipitation with Mars Express. *Journal of Geophysical Research: Space Physics*, *120*(8), 6749–6765. https://doi.org/10.1002/2015ja021150

Gray, C., Chanover, N., Slanger, T., & Molaverdikhani, K. (2014). The effect of solar flares, coronal mass ejections, and solar wind streams on Venus' 5577 Å oxygen green line. *Icarus*, *233*, 342–347. https://doi.org/10.1016/j.icarus.2014.01.029

Gray, C., Peter, K., Pätzold, M., Tellmann, S., Nordheim, T., Schmidt, C., et al. (2025). Venus' O 5577 Å oxygen green line: A global diffuse Proton-induced aurora. *Journal of Geophysical Research: Space Physics*, *130*(2), e2024JA032851. https://doi.org/10.1029/2024JA032851

Hedin, A. E., Niemann, H., Kasprzak, W., & Seiff, A. (1983). Global empirical model of the Venus thermosphere. *Journal of Geophysical Research*, *88*(A1), 73–83. https://doi.org/10.1029/ja088ia01p00073

Leblanc, F., Witasse, O., Lilensten, J., Frahm, R. A., Safaenili, A., Brain, D. A., et al. (2008). Observations of aurorae by SPICAM ultraviolet spectrograph on board Mars Express: Simultaneous ASPERA-3 and MARSIS measurements. *Journal of Geophysical Research (Space Physics)*, *113*(A8), 8311. https://doi.org/10.1029/2008JA013033

Luhmann, J. (1986). The solar wind interaction with Venus. *Space Science Reviews*, *44*(3–4), 241–306. https://doi.org/10.1007/bf00200818

Luhmann, J., & Cravens, T. (1991). Magnetic fields in the ionosphere of Venus. *Space Science Reviews*, *55*(1–4), 201–274. https://doi.org/10.1007/978-94-011-3300-5_4

Luhmann, J., Elphic, R., Russell, C., Slavin, J., & Mihalov, J. (1981). Observations of large-scale steady magnetic fields in the nightside Venus ionosphere and near wake. *Geophysical Research Letters*, *8*(5), 517–520. https://doi.org/10.1029/gl008i005p00517

Martinez, A., Lebonnois, S., Millour, E., Pierron, T., Moisan, E., Gilli, G., & Lefèvre, F. (2023). Exploring the variability of the Venusian thermosphere with the IPSL Venus GCM. *Icarus*, *389*, 115272. https://doi.org/10.1016/j.icarus.2022.115272

Mauk, B. H., Clark, G., Gladstone, G. R., Kotsiaros, S., Adriani, A., Allegrini, F., et al. (2020). Energetic particles and acceleration regions over Jupiter's polar cap and main aurora: A broad overview. *Journal of Geophysical Research: Space Physics*, *125*(3), e2019JA027699. https://doi.org/10.1029/2019ja027699

Mauk, B. H., Haggerty, D., Paranicas, C., Clark, G., Kollmann, P., Rymer, A., et al. (2017). Discrete and broadband electron acceleration in Jupiter's powerful aurora. *Nature*, *549*(7670), 66–69. https://doi.org/10.1038/nature23648

Phillips, J., Stewart, A., & Luhmann, J. (1986). The Venus ultraviolet aurora: Observations at 130.4 nm. *Geophysical Research Letters*, *13*(10), 1047–1050. https://doi.org/10.1029/gl013i010p01047

Soret, L., Gérard, J.-C., Libert, L., Shematovich, V. I., Bisikalo, D. V., Stiepen, A., & Bertaux, J.-L. (2016). SPICAM observations and modeling of Mars aurorae. *Icarus*, *264*, 398–406. https://doi.org/10.1016/j.icarus.2015.09.023

Soret, L., Gérard, J.-C., Schneider, N., Jain, S., Milby, Z., Ritter, B., et al. (2021). Discrete aurora on mars: Spectral properties, vertical profiles, and electron energies. *Journal of Geophysical Research: Space Physics*, *126*(10), e2021JA029495. https://doi.org/10.1029/2021ja029495

Svedhem, H., Titov, D., McCoy, D., Lebreton, J.-P., Barabash, S., Bertaux, J.-L., et al. (2007). Venus Express—The first European mission to Venus. *Planetary and Space Science*, *55*(12), 1636–1652. https://doi.org/10.1016/j.pss.2007.01.013

Weber, T., Brain, D., Mitchell, D., Xu, S., Connerney, J., & Halekas, J. (2017). Characterization of low-altitude nightside Martian magnetic topology using electron pitch angle distributions. *Journal of Geophysical Research: Space Physics*, *122*(10), 9777–9789. https://doi.org/10.1002/2017JA024491

Xu, S., Frahm, R. A., Ma, Y., Luhmann, J. G., & Mitchell, D. L. (2021). Magnetic topology at Venus: New insights into the Venus Plasma environment. *Geophysical Research Letters*, *48*(19), e2021GL095545. https://doi.org/10.1029/2021gl095545

Xu, S., Frahm, R. A., Ma, Y., Luhmann, J. G., Mitchell, D. L., & Persson, M. (2023). Statistical mapping of magnetic topology at Venus. *Journal of Geophysical Research: Space Physics*, *128*(12), e2023JA032133. https://doi.org/10.1029/2023JA032133

Xu, S., Liemohn, M., Bougher, S., & Mitchell, D. (2016). Martian high-altitude photoelectrons independent of solar zenith angle. *Journal of Geophysical Research: Space Physics*, *121*(4), 3767–3780. https://doi.org/10.1002/2015JA022149

Xu, S., Mitchell, D., Liemohn, M., Fang, X., Ma, Y., Luhmann, J., et al. (2017). Martian low-altitude magnetic topology deduced from MAVEN/SWEA observations. *Journal of Geophysical Research: Space Physics*, *122*(2), 1831–1852. https://doi.org/10.1002/2016JA023467

Xu, S., Mitchell, D. L., McFadden, J. P., Fillingim, M. O., Andersson, L., Brain, D. A., et al. (2020). Inverted-V electron acceleration events concurring with localized Auroral observations at Mars by MAVEN. *Geophysical Research Letters*, *47*(9), e2020GL087414. https://doi.org/10.1029/2020GL087414

Xu, S., Mitchell, D. L., McFadden, J. P., Schneider, N. M., Milby, Z., Jain, S., et al. (2022). Empirically determined auroral electron events at Mars–MAVEN observations. *Geophysical Research Letters*, *49*(6), e2022GL097757. https://doi.org/10.1029/2022GL097757

Xu, S., Mitchell, D. L., Whittlesey, P., Rahmati, A., Livi, R., Larson, D., et al. (2024). Closed magnetic topology in the Venusian magnetotail and ion escape at Venus. *Nature Communications*, *15*(1), 6065. https://doi.org/10.1038/s41467-024-50480-0

Xu, S., Weber, T., Mitchell, D. L., Brain, D. A., Mazelle, C., DiBraccio, G. A., & Espley, J. (2019). A technique to infer magnetic topology at Mars and its application to the terminator region. *Journal of Geophysical Research: Space Physics*, *124*(3), 1823–1842. https://doi.org/10.1029/2018ja026366

Zhang, T., Baumjohann, W., Delva, M., Auster, H.-U., Balogh, A., Russell, C., et al. (2006). Magnetic field investigation of the Venus plasma environment: Expected new results from Venus Express. *Planetary and Space Science*, *54*(13–14), 1336–1343. https://doi.org/10.1016/j.pss.2006.04.018